Journal of Photochemistry and Photobiology A: Chemistry 222 (2011) 343–350

Contents lists available at ScienceDirect

Journal of Photochemistry and Photobiology A: Chemistry

journal homepage: www.elsevier.com/locate/jphotochem

Synthesis and photophysical properties of a novel zinc photosensitizer and its gold nanoparticle conjugate

Sharon Moeno, Edith Antunes, Tebello Nyokong*

Department of Chemistry, Rhodes University, Grahamstown 6140, South Africa

ARTICLE INFO

Article history:
Received 10 February 2011
Received in revised form 28 May 2011
Accepted 12 July 2011
Available online 23 July 2011

Keywords:
Phthalocyanine
1,6-Hexanedithiol
Gold nanoparticles
Triplet state quantum yields
Fluorescence lifetimes

ABSTRACT

The peripherally tetra substituted zinc phthalocyanine with 1,6-hexanedithiol as substituent (THdTZnPc, **3**) was synthesized and is reported for the first time in this work. The potential of this zinc complex as a suitable photosensitizer for use in photodynamic therapy was determined through the investigation of the photophysical and photochemical properties. In this work complex **3** is attached to gold nanoparticles through the terminal thiol groups of the phthalocyanine resulting in a **3**-AuNP conjugate whose photophysicochemical properties are investigated. Fluorescence lifetimes were determined using time correlated single photon counting and they show an increase in the abundance of the monomeric species (τ_2) for the Pc in the **3**-AuNP conjugate: ~1 and 0.71 (with respective lifetimes 2.69 ns and 2.86 ns) compared to the free complex **3** with abundances of 0.12 and 0.13 (with respective lifetimes 3.36 ns and 3.28 ns) in DMSO and DMF, respectively.

1. Introduction

Gold nanoparticles (AuNPs) have found application in various fields such as in catalysis, imaging, chemical recognition and photothermal therapy [1–4]. The prominence of these AuNPs results from their intrinsic size tunable optical properties. These optical properties are influenced by the size and shape of the nanoparticle [5,6]. Functionalization of AuNPs with photoactive complexes has been reported [7]. There are many varied photoactive molecules that may be employed for AuNP modification, however in this work the emphasis is on phthalocyanine (Pc) complexes. Phthalocyanines are adaptable macrocyclic complexes that find use as dyes, sensors, in non linear optics and in photodynamic therapy (PDT) of cancer [8–11].

The photophysicochemical properties of Pcs may be altered by simply varying the central metal ion, the axial ligand on the metal ion and the substituents on the periphery of the Pc [11,12]. Diamagnetic ions with a closed shell such as Zn^{2+} and Si^{4+} result in both high triplet quantum yields (Φ_T) and long triplet lifetimes (τ_T) [9,12,13]. The inherent insolubility of Pcs can be improved by introducing a variety of substituents that have the capacity to enhance the solubility of these complexes [14–16]. In addition, introducing substituents onto the periphery of the Pc ring results in considerable changes in the photophysicochemical and spectral properties of phthalocyanine complexes [14–18].

The formation of self assembled monolayers (SAMs) of metallophthalocyanine (MPc) molecules onto bulk gold or AuNP surfaces has been reported [19,20]. In this work AuNPs functionalized with alkyl thio substituted ZnPc are investigated for their potential use in PDT since reports have shown that the AuNPs enhance singlet oxygen production by the Pc [19].

The stabilization of AuNPs by a mono thiol substituted zinc phthalocyanine has been reported [21], and were shown to generate singlet oxygen with enhanced quantum yields as compared to the free Pc. The current work reports on the stabilization of AuNPs using tetrakis-2,(3)-[(1,6-hexanedithiol)phthalocyaninato]zinc(II), (THdTZnPc, **3**, Scheme 1). The complex is tetrasubstituted with thiol groups and also bridged with sulfur. The photophysicochemical behaviour of the complex in the presence and absence of AuNPs is discussed. It has been reported before that for MPc complexes linked to other nanoparticles such as quantum dots [22,23], both the triplet quantum yield and lifetime increase in the presence of nanoparticles, this is very beneficial for use of MPc complexes as photosensitizers. These types of studies have not been reported for AuNP–MPc conjugates, hence the current work. Studies on the ability of noble metal nanoparticles to absorb light in the near-infrared (NIR) region and initiate cancer cell death *via* a photothermal effects are of current interest [24]. Thus the study of phthalocyanines (as photosensitizers for PDT) in the presence AuNPs is part of efforts in developing combination therapy agents where two or more substances are applied for curing one disease, in this case cancer.

* Corresponding author. Tel.: +27 46 6038260; fax: +27 46 6225109.
E-mail address: t.nyokong@ru.ac.za (T. Nyokong).

1010-6030/$ – see front matter © 2011 Elsevier B.V. All rights reserved.
doi:10.1016/j.jphotochem.2011.07.007

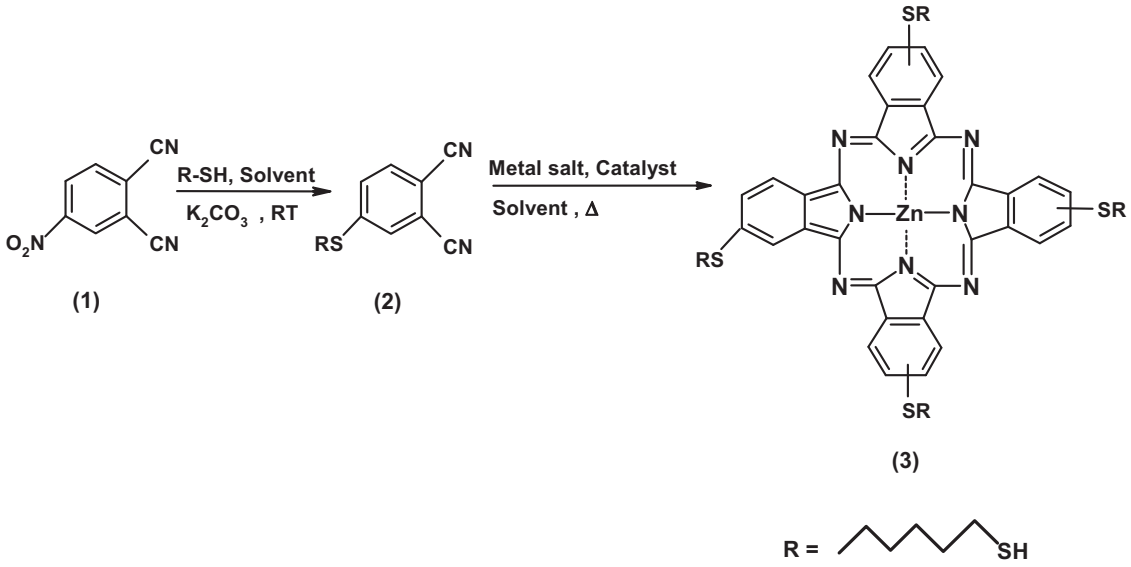

Scheme 1. Synthetic route of 1,6-hexanedithiol (R-SH) tetra substituted zinc phthalocyanine (THdTZnPc, **3**) complex.

2. Experimental

2.1. Materials

Zinc phthalocyanine (ZnPc), 1,3-diphenylisobenzofuran (DPBF), 1,8-diazabicyclo[5,4,0]undec-7-ene (DBU), 1,6-hexanedithiol and gold(III) chloride trihydrate (99.9%) were obtained from Sigma Aldrich. Ethanol, chloroform, dichloromethane (DCM), tetrahydrofuran (THF), toluene, dimethyl formamide (DMF), diethylether, 4-nitrophthalonitrile and acetone were obtained from Saarchem. Tetraoctyl ammonium bromide (TOAB) (98%), sodium borohydride and dimethyl sulfoxide (DMSO) were obtained from Fluka. Biobeads S-X1 were obtained from Bio-Rad. AuNPs were synthesized, purified and characterized according to literature [25]. Ultra pure water was obtained from a Milli-Q Water System (Millipore Corp, Bedford, MA, USA).

2.2. Equipment

Fluorescence excitation and emission spectra were recorded on a Varian Eclipse spectrofluorimeter. UV–visible spectra were recorded on a Varian 500 UV–Vis/NIR spectrophotometer. IR data was obtained by using the Perkin-Elmer spectrum 2000 FTIR Spectrometer. ^{1}H NMR spectra were recorded using a Bruker AMX 400 MHz spectrometer. Elemental analyses were carried out on a Vario EL III MicroCube CHNS Analyzer.

Laser flash photolysis experiments were performed with light pulses produced by a Quanta-Ray Nd:YAG laser providing 400 mJ, 9 ns pulses of laser light at 10 Hz, pumping a Lambda-Physik FL3002 dye (Pyridin 1 dye in methanol). Single pulse energy ranged from 2 to 7 mJ. The analyzing beam source was from a Thermo Oriel xenon arc lamp, and a photomultiplier tube was used as a detector. Signals were recorded with a digital real-time oscilloscope (Tektronix TDS 360). The triplet life times were determined by exponential fitting of the kinetic curves using the program OriginPro 7.5.

X-ray powder diffraction patterns were recorded on a Bruker D8, Discover equipped with a proportional counter, using Cu-Kα radiation (λ = 1.5405 Å, nickel filter). Data were collected in the range from $2\theta = 5^\circ$ to 60°, scanning at 1° min^{-1} with a filter time-constant of 2.5 s per step and a slit width of 6.0 mm. Samples were placed on a silicon wafer slide. The X-ray diffraction data were treated using the freely-available Eva (evaluation curve fitting) software. Baseline correction was performed on each diffraction pattern by subtracting a spline fitted to the curved background and the full-width at half-maximum values used in this study were obtained from the fitted curves. Transmission electron microscope (TEM) images were obtained using a JEOL JEM 1210 transmission electron microscope at 100 kV accelerating voltage. A few drops of the solutions of the samples were placed on carbon coated 300 mesh grids and were left to dry for about 30 s.

Fluorescence lifetimes were measured using a time correlated single photon counting (TCSPC) setup (FluoTime 200, Picoquant GmbH). The excitation source was a diode laser (LDH-P-C-485 with 10 MHz repetition rate, 88 ps pulse width). Fluorescence was detected under the magic angle with a peltier cooled photomultiplier tube (PMT) (PMA-C 192-N-M, Picoquant) and integrated electronics (PicoHarp 300E, Picoquant GmbH). A monochromator with a spectral width of about 8 nm was used to select the required emission wavelength band. The response function of the system, which was measured with a scattering Ludox solution (DuPont), had a full width at half-maximum (FWHM) of about 300 ps. The ratio of stop to start pulses was kept low (below 0.05) to ensure good statistics. All luminescence decay curves were measured at the maximum of the emission peak. The data were analysed with the program FluoFit (Picoquant). The support plane approach was used to estimate the errors of the decay times [26]. Mass spectra data were collected with a Bruker AutoFLEX III Smartbeam TOF/TOF Mass spectrometer. The instrument was operated in positive ion mode using an m/z range of 400–3000. The voltage of the ion sources were set at 19 and 16.7 kV for ion sources 1 and 2 respectively, while the lens was set at 8.50 kV. The reflector 1 and 2 voltages were set at 21 and 9.7 kV, respectively. The spectra were acquired using dithranol as the MALDI matrix, using a 354 nm nitrogen laser.

2.3. Photophysical studies

2.3.1. Fluorescence quantum yield determinations

Fluorescence quantum yields (Φ_F) were determined by a comparative method using Eq. (1) [27]:

$$\Phi_F = \Phi_{F(Std)} \frac{FA_{Std} n^2}{F_{Std} A n_{Std}^2} \quad (1)$$

where F and F_{Std} are the areas under the fluorescence curves of the ZnPc derivative and the reference, respectively. A and A_{Std} are the absorbances of the sample and reference at the excitation wavelength, and n and n_{Std} are the refractive indices of solvents used for the sample and standard, respectively. ZnPc in DMSO was used as a standard, $\Phi_F = 0.20$, for the determination of fluorescence quantum yields [28]. The sample and the standard were both excited at the same relevant wavelength. The fluorescence quantum yield for the MPc complex is represented as $\Phi_{F(\mathrm{MPc})}$ (where MPc represents complex **3**). Solution for fluorescence quantum yield determinations were not deaerated.

2.3.2. Triplet state quantum yields and lifetimes

Triplet quantum yields were determined using a comparative method based on triplet decay, using Eq. (2) [29]:

$$\Phi_T^{Sample} = \Phi_T^{Std} \frac{\Delta A_T^{Sample} \varepsilon_T^{Sample}}{\Delta A_T^{Std} \varepsilon_T^{Sample}} \quad (2)$$

where ΔA_T^{Sample} and ΔA_T^{Std} are the changes in the triplet state absorbance of the ZnPc derivative and the standard, respectively. ε_T^{Sample} and ε_T^{Std} are the triplet state extinction coefficients for complex **3** and standard (ZnPc), respectively. Φ_T^{Std} is the triplet state quantum yield for the standard, ZnPc in DMSO, $\Phi_T^{Std} = 0.65$ [30] and in DMF, $\Phi_T^{Std} = 0.58$ [31]. Φ_T values were determined for complex **3** and are represented as $\Phi_{T(\mathrm{MPc})}$ and the corresponding triplet lifetime as $\tau_{T(\mathrm{MPc})}$.

Quantum yields of internal conversion (Φ_{IC}) were obtained from Eq. (3). This equation assumes that only three processes (fluorescence, intersystem crossing and internal conversion), jointly deactivate the excited singlet state of the ZnPc derivative.

$$\Phi_{IC} = 1 - (\Phi_F + \Phi_T) \quad (3)$$

2.3.3. Singlet oxygen quantum yields

The singlet oxygen quantum yield (Φ_Δ) determinations for **3** were carried out using an experimental set-up that is described in detail elsewhere [32]. In this work Φ_Δ values were determined using DPBF as a singlet oxygen quencher in organic media employing Eq. (4) [33,34]:

$$\Phi_\Delta = \Phi_\Delta^{Std} \frac{W_{\mathrm{DPBF}} \cdot I_{abs}^{Std}}{W_{\mathrm{DPBF}}^{Std} \cdot I_{abs}} \quad (4)$$

where Φ_Δ^{Std} is the singlet oxygen quantum yield for the standard, ZnPc $\Phi_\Delta^{Std} = 0.67$ in DMSO [34] and ZnPc $\Phi_\Delta^{Std} = 0.56$ in DMF [35]. W_{DPBF} and W_{DPBF}^{Std} are the DPBF photobleaching rates in the presence of the ZnPc derivative under investigation and the standard, respectively. I_{abs} and I_{abs}^{Std} are the rates of light absorption by the ZnPc derivative and the standard, respectively. The initial DPBF concentrations used were kept the same for both the ZnPc derivative and the standard.

The values of the fraction of the excited triplet state quenched by ground state molecular oxygen (S_Δ) were determined by employing Eq. (5):

$$S_\Delta = \frac{\Phi_\Delta}{\Phi_\Delta} \quad (5)$$

2.4. Synthesis

2.4.1. 4-(1,6-Hexanedithiol) phthalonitrile (**2**, Scheme 1)

1,6-Hexanedithiol (1.6 mL, 11 mmol) and 4-nitrophthalonitrile (1.68 g, 9 mmol) were dissolved in DMF (80 mL) under a stream of nitrogen and the mixture stirred at room temperature for 15 min. Thereafter, finely ground K_2CO_3 (2.12 g, 15 mmol) was added portion wise over a period of 4 h and the reaction mixture left to stir for a further 24 h at room temperature. The mixture was then added to water (150 mL) and stirred for 30 min. The resulting precipitate was filtered off, thoroughly washed with diethyl ether and acetone, dried and recrystallized from an ethanol. Yield: 2.7 g (90%) IR [(KBr) $\nu_{\max}/\mathrm{cm}^{-1}$]: 3007 (C–H), 2230 (C≡N), 1668, 1583 (C=C), 1437, 1408, 1387 (C–H) 884, 666 (C–S–C). ^{1}H NMR (600 MHz, DMSO-d_6) δ ppm: 7.64–7.62 (m, 1H, Ar–H), 7.53 (d, 1H, Ar–H), 7.48–7.47 (dd, 1H, Ar–H), 3.02–3.00 (m, 12H, methine–H).

2.4.2. Tetrakis-2,(3)-[(1,6-hexanedithiol) phthalocyaninato]zinc(II) (THdTZnPc, **3**, Scheme 1)

A mixture of anhydrous zinc(II) acetate (0.51 g, 2.8 mmol), 4-(1,6-hexanedithiol)phthalonitrile (**2**) (0.5 g, 1.6 mmol), DBU (0.55 mL, 4 mmol) and pentanol (15 mL) was stirred at 160 °C for 5 h. After cooling, the solution was mixed with n-hexane. The green solid product was precipitated and collected by filtration and washed with n-hexane. The crude product was purified by column chromatography using silica gel and eluting with chloroform. Yield: 0.048 g (12%) UV/vis (DMSO): $\lambda_{\max}$ nm; 706 (4.64), 638 (4.08), 364 (4.33). IR (KBr): $\nu_{\max}/\mathrm{cm}^{-1}$; 2997 (C–H), 1436, 1406 (C=C), 1307 (C–H), 667 (C–S–C). ^{1}H NMR (600 MHz, DMSO-d_6) δ ppm: 7.70–7.69 (dd, 4H, Ar–H), 7.53–7.51 (dd, 4H, Ar–H), 6.97 (s, 4H, Ar–H), 4.30–4.11 (m, 48H, Methyl–H), not observed (s, 4H, S–H). Calc. for $C_{56}H_{64}N_8S_8Zn$: C; 57.38, H; 5.59, N; 9.56, Found: C; 57.35, H; 5.44, N; 9.65. MALDI-TOF-MS m/z: Calc.; 1171.08 Found: 1170.56 $[M]^+$ for $C_{56}H_{64}N_8S_8Zn$.

2.4.3. Tetrakis-2,(3)-[(1,6-hexanedithiol) phthalocyaninato]zinc(II) functionalized AuNPs (**3**-AuNP, Scheme 2)

The THdTZnPc (**3**) (0.020 g, 0.016 mmol) and TOAB-AuNPs (0.050 g) in toluene (5 mL) were mixed and stirred for 72 h for the ligand exchange to take place so as to attach the Pc onto AuNPs. After the ligand exchange, the unreacted MPc was separated in a size exclusion column: Biobeads S-X1 using toluene as an eluent. The MPc–AuNP conjugate comes off first, followed by unreacted AuNPs and finally the unreacted MPc. IR [(KBr) $\nu_{\max}/\mathrm{cm}^{-1}$]: 3018 (N–H), 2932 (C–H), 1517 (C=C), 1213 (C–N), 1039 (C–C), 749, 667 (N–H).

2.5. AuNP and **3**-AuNP characterization

The synthesis of AuNPs and their characterization has been reported before [21]. The sizes of the TOAB AuNPs and the MPc functionalized AuNPs were determined using X-ray powder diffraction (XRD) [36].

XRD allows the determination of the particle-diameter (d) through the use of the Debye–Scherrer Eq. (6):

$$d(\mathring{A}) = \frac{k\lambda}{\beta \ \mathrm{Cos}\,\theta} \quad (6)$$

where k is an empirical constant equal to 0.9, λ is the wavelength of the X-ray source, (1.5405 Å), β is the full width at half maximum of the diffraction peak, and θ is the angular position of the peak.

3. Results and discussion

3.1. Characterization of complex **3**

The new complex (**3**) was characterized using UV–vis, IR, NMR spectroscopies, MALDI-TOF mass spectra and elemental analysis. The analyses are all consistent with the expected as shown in the experimental section. The complex exhibited moderate solubility in organic solvents such as $CHCl_3$, DCM, THF, DMF and DMSO.

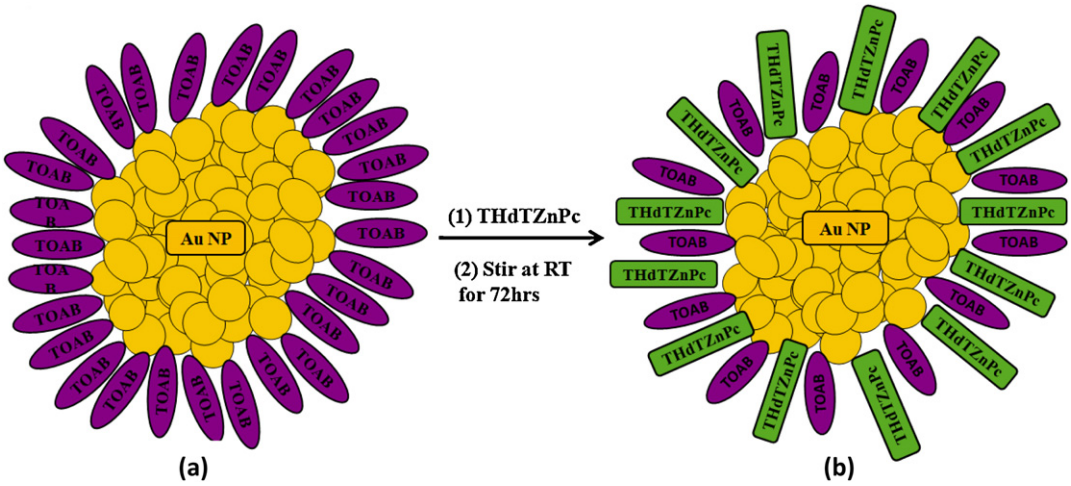

Scheme 2. A schematic representation of the functionalization of TOAB AuNPs with complex **3** (THdTZnPc, **3**, b), not a true representation of the loading capacity of Pc onto the AuNPs.

The mass spectra of the phthalocyanine was obtained by the relatively soft ionization MALDI-TOF technique with the molecular ion peak observed at 1170.56 for (**3**).

The ^{1}H NMR spectra of the ZnPc derivative (**3**) shows complex patterns due to the mixed isomer character of tetra substituted MPc derivatives and also due to aggregation. Complex **3** was found to be pure by ^{1}H NMR with all the substituents and ring protons were observed in their respective regions.

The newly synthesized complex **3** showed slight aggregation in the absorbance spectra, Fig. 1a(i) and b(i), with Q band maxima at 702 in chloroform. The broad feature at 770 nm in chloroform is most likely due to protonation in acid solvents such as chloroform [37]. The Q band is observed at 706 nm in DMSO and 702 in DMF. The excitation spectra are mirror images of the fluorescence emission spectra, Fig. 2. The absorption spectra is however broad due to aggregation. Table 1 shows the spectral data with Stokes shifts for complex **3** that are typical of Pc complexes in general [38].

The fluorescence quantum yield (Φ_F) values of complex **3** in DMSO and DMF are shown in Table 1 for excitation at 620 nm in both DMSO and DMF. The values are low compared to MPc complexes in general in both DMSO and DMF due to aggregation [38]. Within experimental error, the Φ_F values are not very different in DMF and DMSO.

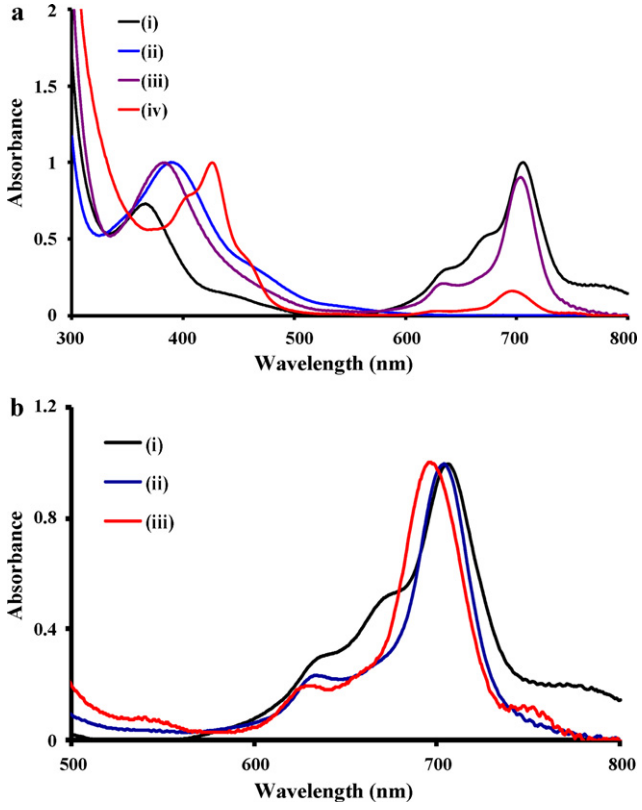

Fig. 1. (a) Absorption spectra of (i) complex **3** alone, (ii) TOAB AuNPs, (iii) mixture of **3** and AuNPs and (iv) **3**-AuNP conjugate in $CHCl_3$. (b) Normalized Q band absorption spectra for (i) complex **3** alone, (ii) mixture of **3** and AuNPs and (iii) **3**-AuNP conjugate in $CHCl_3$.

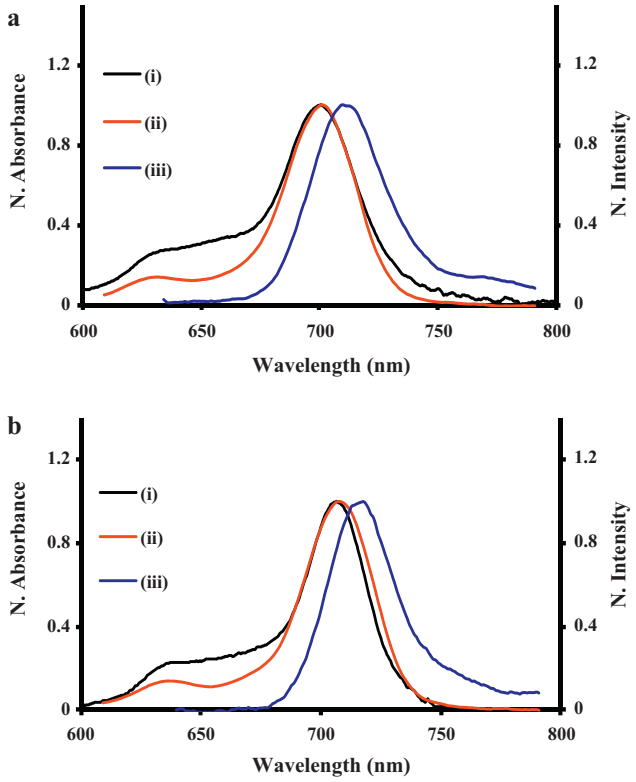

Fig. 2. Absorption (i), excitation (ii) and emission (iii) spectra of complex **3** in (a) DMF and (b) DMSO ($\lambda_{excitation}$ = 620 nm).

Table 1
Absorbance and fluorescence data for complex **3** and **3**-AuNP conjugate.

Sample	Solvent	Q band λ_{max} (nm)	Emission λ_{max} (nm)	Stokes shift $\Delta\lambda_{stokes}$ (nm)	Log ε	$\Phi_{F(MPc)} \pm 0.01$
3	DMSO	706	718	12	4.63	0.06
3-AuNP	DMSO	697	706	9	–	0.07
3	DMF	702	712	10	4.88	0.08
3-AuNP	DMF	696	706	10	–	0.06

3.2. Characterization of complex **3**-AuNP conjugates

XRD diffractograms obtained for this work showed the expected Bragg reflections at 2θ values of 39.1, 45.3 and 65.2 which are assigned to the (1 1 1), (2 0 0), (2 2 0) reflections of cubic face centred nanoparticles. However many other reflections were observed and these may be due to the TOAB stabilizer used on the parent AuNPs as well as local structural disorders and defects of the AuNPs, Fig. 3 [39,40]. The Pc functionalized AuNPs show less Bragg reflections and these as expected are slightly shifted in comparison to those of the parent AuNPs. The sizes were determined for TOAB AuNPs to be 4.96 nm while that of the complex **3** functionalized AuNPs was found to be around 5.96 nm. The functionalization of the AuNPs with the Pc increases the size of the AuNP in the conjugate by 1 nm.

The TOAB AuNPs and the AuNPs functionalized with self assembled monolayers of complex **3** (represented as **5** in Scheme 2) were also characterized with transmission electron microscopy (TEM) [36,41], Fig. 4A and B. These TEM pictures at the same magnification (2000 nm) clearly show the distinction between TOAB AuNPs and **3**-AuNPs, where TOAB stabilized AuNPs are clustered. The **3**-AuNP conjugate particles are monodisperse unlike their non MPc-functionalized counterparts indicative that complex **3** has been successfully attached (assembled) onto the AuNPs.

The MPc substituents in this work each terminate with a thiol moiety. It is this thiol group that allows for attachment onto the AuNPs since they are known to have a high affinity for gold surfaces. Complex **3** has four thiol groups, suggesting a possibility of one or more of the thiol groups to be attached to the AuNPs. It is however more feasible that the Pcs are perpendicularly oriented on the AuNP surface, since the Pc units displace the TOAB stabilizer which could not have easily been displaced to allow for planar orientation of the Pc units across the surface of the AuNP.

The absorbance spectra of complex **3** alone, the mixture of complex **3** and AuNPs and the **3**-AuNP conjugate at the Q band position are shown as normalized spectra in Fig. 1b in $CHCl_3$. The normalized superimposed spectra show that there is a slight shift of the Q-band position from 702 nm for complex **3** alone to 698 nm for complex **3** in the mixture with AuNPs and to 692 nm for complex **3** in the **3**-AuNP conjugate. All the spectral shifts of the Q band position of the Pc are towards the blue in the presence of AuNPs. The absorption spectrum of the Pc in the conjugate (**3**-AuNP) is narrower compared to **3** alone (Fig. 1b). The large blue shifting for **3**-AuNP conjugate shows that the sulfur groups are engaged in the linking to AuNPs.

As observed in Fig. 1b, the absorption spectrum of complex **3** alone (curve i) was rather broad and this behaviour is attributed to aggregation. However, when the solution of AuNPs was added to the solution of complex **3**, the Pc was disaggregated by the AuNPs as judged by the narrowing of the Q band (curve ii). This effect of monomerization of the Pc Q-band is also observed in the conjugate where there is no sign of aggregation of complex **3** in the **3**-AuNP conjugate, Fig. 1b(curve iii). The monomerizing effect of the Pc was shown to be by TOAB. It is suggested that complex **3** attaches to the AuNPs *via* a coordinate covalent bond.

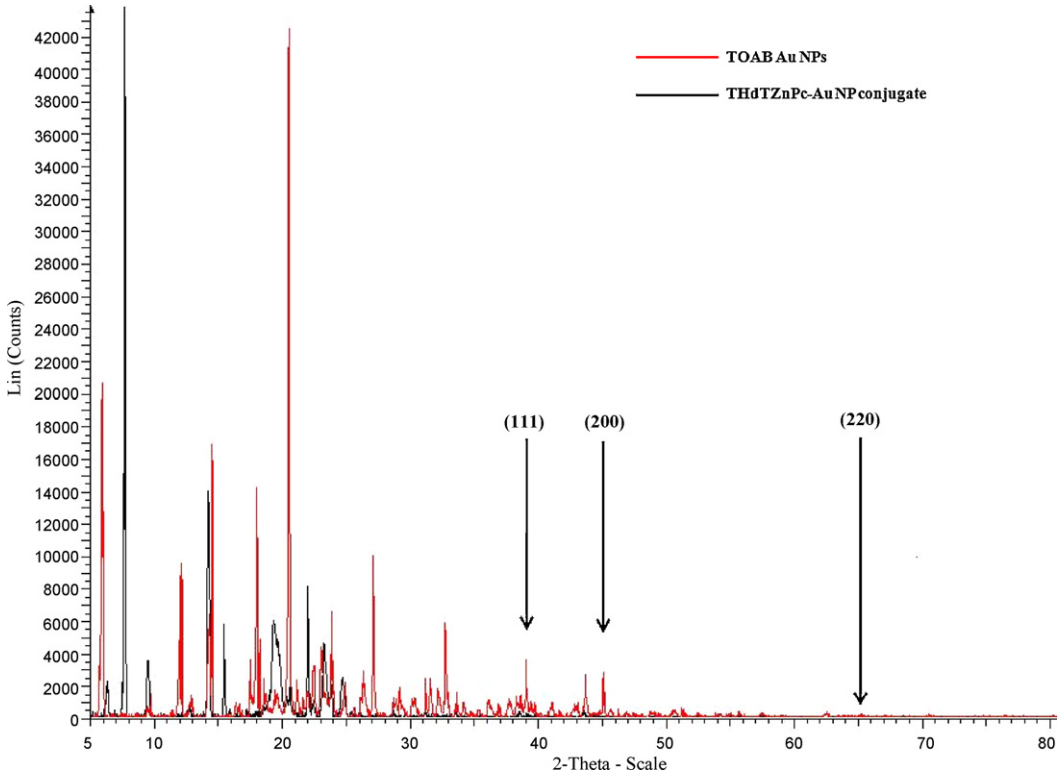

Fig. 3. Overlaid X-ray diffractograms of TOAB stabilized AuNPs and the **3**-AuNP conjugate.

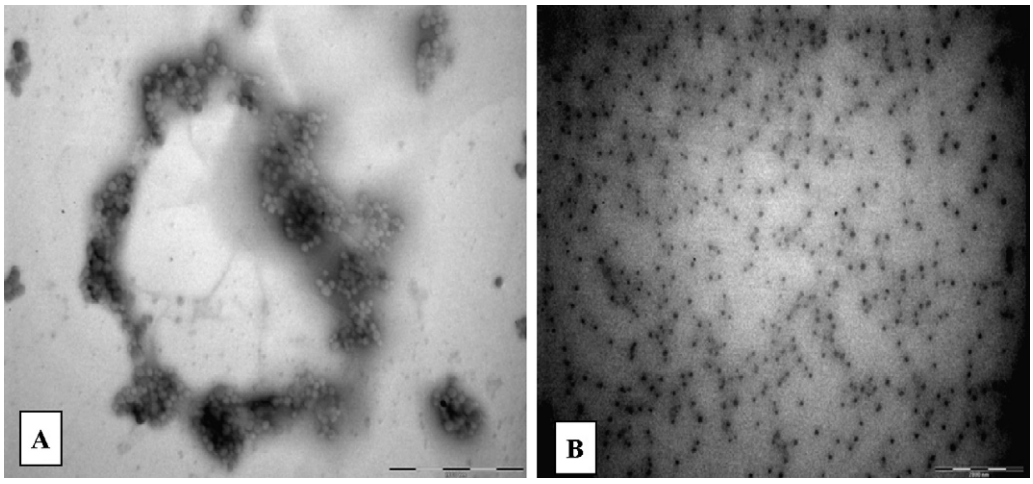

Fig. 4. TEM images of (A) TOAB stabilized AuNPs (4.96 nm) and (B) **3**-AuNPs (5.96 nm) (the scale bar for A and B is 2000 nm).

The emission of complex **3** attached to the AuNPs was slightly blue-shifted compared to that of free complex **3** (shown in Fig. 5) in DMSO and DMF. The Φ_F values of complex **3** in the **3**-AuNP conjugate in DMSO and DMF are shown in Table 1. It is expected that for the MPc molecules in the **3**-AuNP conjugate, the AuNPs will quench the emission of the Pc hence lowering the Φ_F values, but Table 1 shows no significant decrease in these values in the presence of AuNPs.

In Fig. 1a the surface plasmon band for TOAB AuNPs is shown to be around 389 nm in $CHCl_3$. However this band is merged with the B band of phthalocyanines with a maximum at 426 nm for the **3**-AuNP conjugate also in $CHCl_3$. The change in the surface plasmon absorption band is indicative of modification of NPs. The observed spectral changes for the gold nanoparticle surface plasmon band in the **3**-AuNP conjugate (Fig. 1a) indicate that the attachment of the complex **3** to the AuNPs was successful and that it affects the size of the nanoparticles as proven with XRD. The absorbance of the mixture of AuNPs with complex **3** shows the resulting merger of the B-band of the Pc with the surface plasmon band of the AuNPs with the peak from this combination appearing at 384 nm in $CHCl_3$.

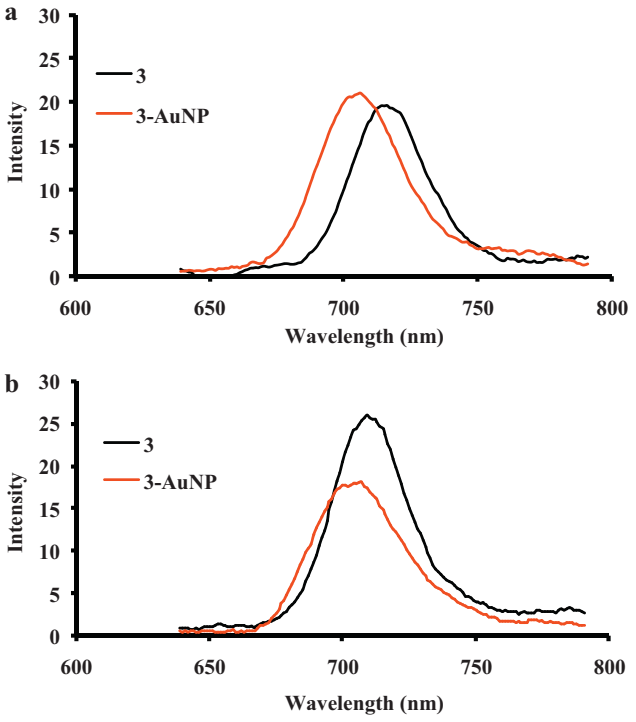

Fig. 5. Emission spectra of complex **3** and **3**-AuNP conjugate in (a) DMSO and (b) DMF ($\lambda_{excitation}$ = 620 nm).

Table 2
Fluorescence lifetime measurements for complex **3** and **3**-AuNP conjugate in DMSO and DMF.

Sample	τ_1 (ns)[a]	α_1[b]	τ_2 (ns)[a]	α_2[b]
3 (DMSO)	1.88 ± 0.01	0.88	3.36 ± 0.04	0.12
3-AuNP (DMSO)	0.001 ± 0.0	0.002	2.69 ± 0.03	0.998
3 (DMF)	2.04 ± 0.01	0.87	3.28 ± 0.03	0.13
3-AuNP (DMF)	0.95 ± 0.01	0.29	2.86 ± 0.03	0.71

[a] Fluorescence lifetimes at MPc emission.
[b] α denotes the amplitude fraction.

3.3. Fluorescence lifetimes

Time correlated single photon counting (TCSPC) measurements were carried out at the MPc emission maxima. The measurements reveal biexponential decay kinetics for complex **3**, Fig. 6, which is common for substituted Pc macrocycles especially those having monomeric and aggregated species. The results are shown in Table 2, where the aggregated specie of the Pc displays shorter fluorescence lifetime τ_1 while the monomeric specie exhibits longer fluorescence lifetime τ_2. Complex **3** showed a trend where the aggregated specie (with τ_1) was in larger abundance in both DMSO and DMF for the MPc alone. The abundance changed though, in the **3**-AuNP conjugate because as seen from Table 2 the aggregated specie (τ_1) was now in less abundance in DMF and DMSO. The fact that the abundance of the monomeric species of complex **3** is increased in the **3**-AuNP conjugate solutions (compared to complex **3** alone) confirms that the AuNPs and the associated TOAB stabilizer have a monomerizing effect on the phthalocyanine complex in solution. It is reasonable to expect disaggregation of complex **3** to be a cause for the increased abundances of the monomeric species (τ_2) in the conjugate as was clearly observed in Fig. 1b.

There was a lowering of the MPc lifetimes in the conjugate compared to those of complex **3** alone in solution. This observation of lowered τ_2 values may be due to the interaction of the AuNPs and complex **3** which could possibly result in energy transfer from the AuNPs to complex **3**, but this is tentative since TCSPC measurements were carried out at the excitation wavelength where only complex **3** absorbs. Two main mechanisms for energy transfer are well known with one being that of the Förster resonance energy transfer. This mechanism, however would mainly involve excita-

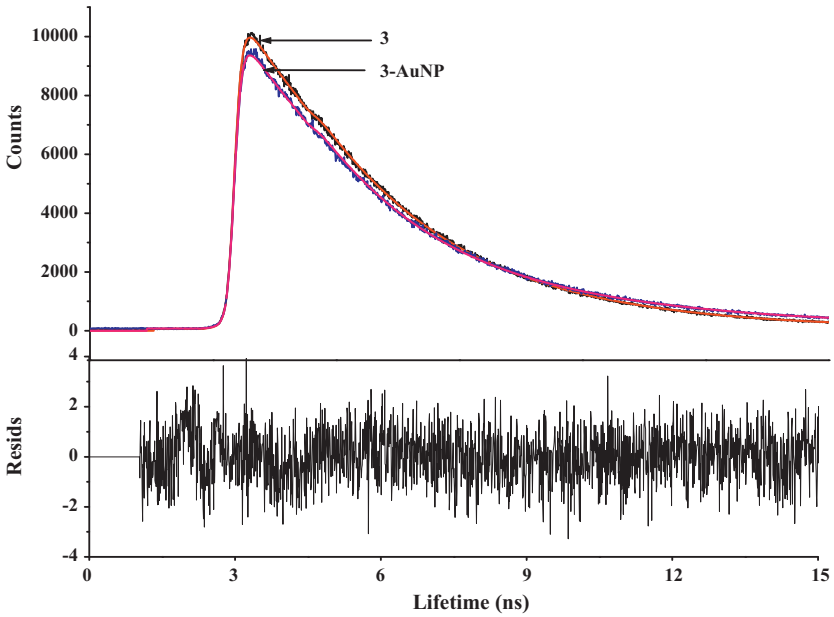

Fig. 6. Photoluminescence decay curves of (i) complex **3** alone and (ii) **3**-AuNP conjugate in DMF ($\lambda_{excitation}$ = 712 nm, $\tau_{1/e}$ = 3.28 and 2.86 ns, respectively).

tion at the AuNP emission wavelength and thus is not possible in this work. Another principal mechanism for energy transfer is the Dexter energy transfer which requires very short distance ranges (<1 nm) which are possible for complex **3** assembled onto the AuNPs (conjugate) [26]. Dexter energy transfer proceeds through electron transfer and is most likely to take precedence in this work considering the fact that electron and charge transfer are prone to occur in the complex **3** and AuNP conjugates [20,26].

3.4. Triplet state quantum yields (Φ_T) and lifetime (τ_T) studies

Eq. (2) was used to calculate for Φ_T values. The Φ_T values quantify the fraction of absorbing molecules that undergo intersystem crossing (ISC) to the triplet state. In Fig. 7 a representative triplet state decay curve for complex **3** in DMF is shown. A variation of Φ_T values of complex **3** and for **3** in the **3**-AuNP conjugate in DMSO and DMF is shown in Table 3. An increase of the Φ_T values for complex **3** in the **3**-AuNP conjugate was observed. This observation results from the heavy atoms of AuNPs which encourage intersystem crossing (to the triplet state) of the MPc complex through spin orbit coupling. The increase in Φ_T values of MPcs associated with heavy metal ions constituting nanoparticles (CdTe QDs) has been previously reported by our group [42,43]. The slightly lower values

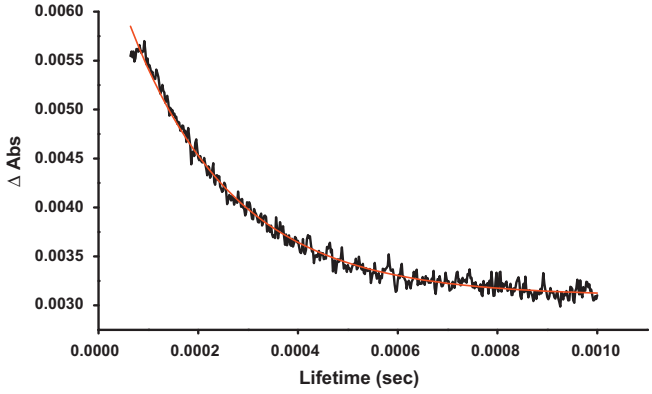

Fig. 7. A representative triplet decay curve for complex **3** ($\lambda_{excitation}$ = 685 nm in DMF).

Table 3
Photophysical parameters for **3** alone and in the **3**-AuNP conjugate.

Sample	Solvent	$\Phi_{T(MPc)}$	$\tau_{T(MPc)}$/μs	Φ_{IC}	Φ_{Δ}	S_{Δ}
3	DMSO	0.67	76	0.27	0.59	0.88
3-AuNP	DMSO	0.80	84	0.13	0.74	0.93
3	DMF	0.63	210	0.29	0.59	0.94
3-AuNP	DMF	0.75	304	0.19	0.71	0.95

in DMF compared to DMSO could be related to lower viscosity of the former. A decrease in viscosity of the solvent increases the possibility of deactivation of the excited state by external conversion, and DMF is less viscous than DMSO.

Triplet state lifetime (τ_T) values of the complex **3** alone were slightly lower than those of complex **3** assembled onto AuNPs, Table 3. This observation however does not correspond well to the increased Φ_T values in the **3**-AuNP conjugate, where an increase in Φ_T values is expected to result in a decrease in the triplet state lifetime, this behaviour has been encountered with the use of other nanoparticles [22,23,42]. The values of τ_T are much larger in DMF than in DMSO in Table 3; this is not expected based on the above discussion on differences in viscosity between the two solvents. However the high τ_T values correspond to slightly lower Φ_T values for **3** and its conjugate.

The Φ_{IC} values were calculated with the use of Eq. (3). As shown in Table 3, the values of Φ_{IC} for complex **3** were moderate indicative of the fact that radiationless transitions have an important role in the deactivation of the excited state. The combined effect of radiationless transitions and the high Φ_T values account for deactivation of the excited state thereby resulting in the low Φ_F values obtained for complex **3**.

3.5. Singlet oxygen quantum yields

Singlet oxygen quantum yield (Φ_{Δ}) values reflect the amount of singlet oxygen produced. The Φ_{Δ} values were obtained through the use of Eq. (4). The singlet oxygen generation efficiency depends on the triplet state quantum yield Φ_T [23] and the triplet state lifetime τ_T. Table 3 shows that the Φ_{Δ} values for **3** are relatively high in both DMSO and DMF, corresponding to the large Φ_T values. The Φ_{Δ} values of complex **3** in Table 3 are: Φ_{Δ} = 0.59 (DMSO), Φ_{Δ} = 0.59

(DMF) for **3** alone and Φ_Δ = 0.74 (DMSO), Φ_Δ = 0.71 (DMF) for **3** in the **3**-AuNP conjugate. Thus Φ_Δ values for **3** are the same in DMSO and DMF and do not show the trend observed for Φ_T values as expected. The trend for Φ_Δ values for **3**-AuNP follows that observed for Φ_T values when comparing DMSO with DMF.

The fraction of the excited triplet state quenched by ground state molecular oxygen (S_Δ) was calculated using Eq. (5). S_Δ values give the efficiency of energy transfer from the triplet state of the MPc complexes to the ground state of molecular oxygen. S_Δ values close to unity are an indication of a high efficiency of energy transfer. Table 3 shows that the S_Δ values for **3** and the **3**-AuNP conjugate in DMSO and DMF are all close to unity.

4. Conclusions

The synthesis and characterization of tetrakis-2,(3)-[(1,6-hexanedithiol) zinc phthalocyanine] was carried out successfully. The photophysicochemical properties of complex **3** were determined in DMSO and DMF. Complex **3** was successfully assembled onto AuNPs by virtue of the free terminal thiol groups on the substituents of the Pc. The presence of the TOAB stabilizing agent resulted in the monomerization of the complexes in DMSO and DMF but not in chloroform. The photophysicochemical properties of the Pc in the **3**-AuNP conjugate were enhanced. There is an increase in both the triplet yield quantum yields and lifetimes of complex **3** in the presence of AuNPs. The increase in both parameters shows advantage of the conjugates for use as photosensitizers. The fluorescence quantum yields however showed insignificant change in the presence of AuNPs. The fluorescence lifetimes of complex **3** were slightly decreased in the **3**-AuNP conjugate.

Acknowledgements

This work was supported by the Department of Science and Technology (DST) and National Research Foundation (NRF), South Africa through DST/NRF South African Research Chairs Initiative for Professor of Medicinal Chemistry and Nanotechnology as well as Rhodes University and Medical Research Council of South Africa. SM thanks DAAD foundation for a scholarship.

References

[1] M.J. Hostetler, R.W. Murray, Curr. Opin. Colloid Interface 2 (1997) 42.
[2] M. Pelton, J. Aizpurua, G. Bryant, Laser Photon Rev. 2 (2008) 136.
[3] M.-C. Daniel, D. Astruc, Chem. Rev. 104 (2004) 293.
[4] C. Walkey, E.A. Sykes, W.C.W. Chan, Hematology (2009) 701.
[5] K.S. Kim, D. Demerelnyamba, H. Lee, Langmuir 20 (2004) 556.
[6] J.-P. Deng, C. Wu, C.-H. Yang, C.-Y. Mou, Langmuir 21 (2005) 8947.
[7] C-k. Kim, P. Ghosh, V.M. Rotello, Nanoscale 1 (2009) 61.
[8] Stillman, T. Nyokong, in: C.C. Leznoff, A.B.P. Lever (Eds.), Phthalocyanines: Properties and Applications, vol. 1, VCH, New York, 1989 (Chapter 3).
[9] E. Ben-Hur, W.S. Chan, in: K.M. Kadish, K.M. Smith, R. Guilard (Eds.), Porphyrin Handbook, Phthalocyanine Properties and Materials, vol. 19, Academic Press, New York, 2003 (Chapter 117).
[10] D. Dini, M. Hanack, in: K.M. Kadish, K.M. Smith, R. Guilard (Eds.), Porphyrin Handbook, Phthalocyanine Properties and Materials, vol. 17, Academic Press, New York, 2003 (Chapter 107).
[11] I. Okura, Photosensitization of Porphyrins and Phthalocyanines, Gordon and Breach Publishers, Germany, 2001.
[12] K. Ishii, N. Kobayashi, in: K.M. Kadish, K.M. Smith, R. Guilard (Eds.), The Porphyrin Handbook, vol. 16, Elsevier, 2003 (Chapter 1).
[13] A.C. Tedesco, J.C.G. Rotta, C.N. Lunardi, Curr. Org. Chem. 7 (2003) 187.
[14] T. Nyokong, H. Isago, J. Phthalocyanines Porphyrins 8 (2004) 1083.
[15] M. Durmus, T. Nyokong, Photochem. Photobiol. Sci. 6 (2007) 659.
[16] N. Kobayashi, H. Konami, Phthalocyanines: Properties and Applications, vol. 4, VCH, New York, 1999.
[17] W. Chidawanyika, A. Ogunsipe, T. Nyokong, New J. Chem. 31 (2007) 377.
[18] A.W. Snow, in: K.M. Kadish, K.M. Smith, R. Guilard (Eds.), Porphyrin Handbook: Phthalocyanine Properties and Materials, vol. 17, Academic Press, 2003 (Chapter 109).
[19] M. Camerin, M. Magaraggia, M. Soncin, G. Jori, M. Moreno, I. Chambrier, M.J. Cook, D.A. Russell, Eur. J. Cancer 46 (2010) 1910.
[20] A. Kotiaho, R. Lahtinen, A. Efimov, H.K. Metsberg, E. Sariola, H. Lehtivuori, N.V. Tkachenko, H. Lemmetyinen, J. Phys. Chem. C 114 (2010) 162.
[21] D.C. Hone, P.I. Walker, R. Evans-Gowing, S. FitzGerald, A. Beeby, I. Chambrier, M.J. Cook, D.A. Russell, Langmuir 18 (2002) 2985.
[22] J. Ma, J.Y. Chen, M. Idowu, T. Nyokong, J. Phys. Chem. B 112 (2008) 4465.
[23] M. Idowu, J.-Y. Chen, T. Nyokong, New J. Chem. 32 (2008) 290.
[24] X. Huang, P.K. Jain, I.H. El-Sayed, M.A. El-Sayed, Lasers Med. Sci. 23 (2008) 217.
[25] M. Brust, M. Walker, D. Bethell, D.J. Schffrin, R. Whyman, J. Chem. Soc., Chem. Commun. (1994) 801.
[26] J.R. Lakowiecz, Principles of Fluorescence Spectroscopy, Second edition, Kluwer Academic/Plenum Publishers, New York, 1999.
[27] S. Fery-Forgues, D. Lavabre, J. Chem. Educ. 76 (1999) 1260.
[28] A. Ogunsipe, J.-Y. Chen, T. Nyokong, New J. Chem. 28 (2004) 822.
[29] J.H. Brannon, D. Madge, Picosecond laser photophysics. Group 3A phthalocyanines, J. Am. Chem. Soc. 102 (1980) 62.
[30] P. Kubat, J. Mosinger, J. Photochem. Photobiol. A 96 (1996) 93.
[31] J. Kossanyi, D. Chahraoui, Int. J. Photoenergy 2 (2000) 9.
[32] S. Maree, T. Nyokong, J. Porphyrins Phthalocyanines 5 (2002) 782.
[33] A. Ogunsipe, D. Maree, T. Nyokong, J. Mol. Struct. 650 (2003) 131.
[34] N. Kuznetsova, N. Gretsova, E. Kalmykova, E. Makarova, S. Dashkevich, V. Negrimovskii, O. Kaliya, E. Lukyanets, Russ. J. Gen. Chem. 70 (2000) 133.
[35] W. Spiller, H. Kliesch, D. Wohrle, S. Hackbarth, B. Roder, G. Schnurpfeil, J. Porphyrins Phthalocyanines 2 (1998) 145.
[36] E. Jiménez, K. Abderrafi, J. Martínez-Pastor, R. Abargues, J.L. Valdés, R. Ibáñeze, Superlattice Microstruct. 43 (2008) 487.
[37] M. Durmuş, T. Nyokong, Spectrochim. Acta A 69 (2008) 1170.
[38] T. Nyokong, Coord. Chem. Rev. 251 (2007) 1707.
[39] T.G. Schaaff, M.N. Shafigullin, J.T. Khoury, I. Vezmar, R.L. Whetten, W.G. Cullen, P.N. First, C. Gutiérrez-Wing, J. Ascensio, M.J. Jose-Yacamán, J. Phys. Chem. B 101 (1997) 7885.
[40] D.V. Leff, L. Brandt, J.R. Heath, Langmuir 12 (1996) 4723.
[41] Y. Liu, Y-Li. Zhao, Y. Chen, M. Wang, Macromol. Rapid Commun. 26 (2005) 401.
[42] S. Moeno, E. Antunes, S. Khene, C. Litwinski, T. Nyokong, Dalton Trans. 39 (2010) 3460.
[43] W. Chidawanyika, C. Litwinski, E. Antunes, T. Nyokong, J. Photochem. Photobiol. A: Chem. 212 (2010) 27.